Electron trapping centres and cross sections in $LiNbO_3$ studied by ^{57}Co Mössbauer emission spectroscopy

1999 J. Phys.: Condens. Matter 11 6239

(http://iopscience.iop.org/0953-8984/11/32/315)

J. Phys.: Condens. Matter **11** (1999) 6239–6250. Printed in the UK PII: S0953-8984(99)02684-3

Electron trapping centres and cross sections in $LiNbO_3$ studied by ^{57}Co Mössbauer emission spectroscopy

T Becze-Deák†, L Bottyán†, G Corradi‡, L Korecz§, D L Nagy†, K Polgár‡, S Sayed‖ and H Spiering¶

† KFKI Research Institute for Particle and Nuclear Physics, H-1525 Budapest, POB 49, Hungary
‡ Crystal Physics Laboratory, Institute for Solid State Physics and Optics, H-1525 Budapest, POB 49, Hungary
§ Institute of Chemistry, Chemical Research Center, Hungarian Academy of Sciences, H-1525 Budapest, POB 17, Hungary
‖ Al-Azhar University, Cairo, Egypt
¶ Institut für Anorganische Chemie und Analytische Chemie, Johannes Gutenberg Universität, Staudinger Weg 9, D-55099 Mainz, Germany

E-mail: tbecze@rmki.kfki.hu

Received 12 March 1999, in final form 14 June 1999

Abstract. Fast electron trapping processes and aliovalent charge states following the ^{57}Co(EC)^{57}Fe decay are studied in undoped, 5.4 mol% Mg-doped and 0.1 mol% Fe-doped $LiNbO_3$ in various thermochemical reduction (TCR) states. Static ^{57}Co Mössbauer emission spectra of congruent Mg:$LiNbO_3$ recorded at $T = 4.2$ K in external magnetic field of 4.6 T are presented. Trapping cross section ratios are derived for Fe_{Li}^{3+}, Nb_{Li}^{5+} and Mg_{Li}^{2+}. A method to determine trap concentrations for TCR states of $LiNbO_3$ is outlined. The electron-capture distance of the traps is found to be 2.7 ± 1.4 nm. As this is much smaller than the 6 keV Auger-electron penetration depth, it is concluded that the distribution of the aliovalent charge states at 4.2 K is determined mainly by the 600 eV Auger electrons.

1. Introduction

Due to its various applications, in particular in photo-refractive devices, the electronic and optical properties of $LiNbO_3$, as well as the studies of the underlying basic charge trapping processes are of general interest. The composition of $LiNbO_3$ crystals which grow congruently from the melt shows Li-deficiency. It has been a long discussion if and how this deficiency and the consequent atomic defect structure is related to the electronic properties of $LiNbO_3$ and how these properties can be affected by melt-doping of the crystals. Mössbauer emission spectroscopy (MES) offers an excellent possibility for investigating sub-microsecond charge relaxation. This time scale, being of importance in real-time holography, is readily attained by studying aftereffects of decaying radionuclei in insulators and in semiconductor matrices. Although ^{57}Co:$LiNbO_3$ was the subject of several MES investigations [1–7], the mechanism of charge recombination following internal (and external) irradiation effects in $LiNbO_3$ is still puzzling. In the present work we report on anomalous charge states as an aftereffect of electron-capture (EC) decay of the ^{57}Co Mössbauer isotope in congruent $LiNbO_3$. We propose here and test for $LiNbO_3$ a modified quantitative version of the model describing the charge relaxation around the nucleogenic ion (hereafter *Fe) shortly after the ^{57}Co(EC)^{57}Fe

0953-8984/99/326239+12$30.00

decay (model of competing acceptors [8, 9], hereafter MoCA). Based on this, we determine parameters of intrinsic and extrinsic electron acceptors in $LiNbO_3$ prepared with different dopants and in different thermochemical states.

2. The ^{57}Co(EC)^{57}Fe decay and its aftereffects in insulators

In order to perform a ^{57}Co Mössbauer source experiment, the ^{57}Co radionuclei are introduced in the studied matrix by thermal diffusion or by ion implantation. When an EC process from the K- or L-shell of ^{57}Co occurs, the 136.5 keV $5/2^-$ excited state of the newly formed ^{57}Fe daughter nucleus populates. Having a lifetime of 13 ns this decays with 91% probability into the 14.4 keV ($I = 3/2^-$, $\tau = 141$ ns) Mössbauer level of ^{57}Fe. Processes with time scales longer than or comparable to the $\tau = 141$ ns lifetime of the Mössbauer level can be followed by MES.

Within $\sim 10^{-12}$ s after EC, the electron shell of the *Fe is re-organised by fast x-ray and Auger processes, with dominance of the latter. Auger electrons with energies of 5.4–6.2 keV and 550–720 eV are emitted from KLL and LMM transitions, respectively [10]. Eventually, the nucleogenic *Fe is left in a highly ionized state up to 7+ [11]. This results in a variety of chemical and physical aftereffects in the surrounding lattice and in the nucleogenic ion's electron shell [10, 12–16]. In metals, the highly charged ionic state relaxes before the Mössbauer level of the nucleus is populated, but in semiconductors and insulators metastable ionic species have often been observed by MES [2, 17]. Such a thoroughly investigated system was ^{57}Co:CoO [18] where, although Co is a main constituent, beside $^*Fe^{2+}$, a massive 47% $^*Fe^{3+}$ was detected by MES. The presence of $^*Fe^{3+}$ is anomalous, since the initial valence state of cobalt is clearly 2+. MoCA has been successfully applied for CoO [19] to describe the creation of anomalous $^*Fe^{3+}$ after the ^{57}Co(EC)^{57}Fe decay. The sum and substance of MoCA is the following. Assume that the relaxation of the central ion into the $^*Fe^{3+}$ state is finished before the Mössbauer level is populated. Auger electrons, having travelled a distance of the order of the penetration depth (for 5.6 keV electrons $\sim$100 nm [10]) get thermalized in the lattice. Dependent on whether the 'last' electron is re-trapped by the nucleogenic ion or some other electron trap competing with it, $^*Fe^{2+}$ or $^*Fe^{3+}$ is observed in the MES spectrum.

A quantitative version of MoCA was developed by Harami *et al* [20], establishing a relation between the cation vacancy content of the lattice and the amount of $^*Fe^{3+}$ in the MES spectra. Although the qualitative picture of MoCA is probably correct, however, as analysed by Spiering *et al* [10], the model of Harami *et al* [20] has a number of shortcomings. First, it ignores the high number (300–700) of electron–hole pairs created by the Auger electrons along their track in the insulator in the close surroundings of the *Fe. Second, it ignores that, beside the high energy ($\geqslant$5.4 keV) KLL Auger electrons, in about 40% of the events the Auger cascade results only in $\sim$600 eV LMM Auger electrons. The typical penetration radius of the LMM electrons however, is much smaller than that of the KLL Auger electrons (only $\sim$11 nm [21]).

Due to the low concentration of ^{57}Co, there is either no, or only one, decay at a certain time in the capture volume. The probability ratio r of having $^*Fe^{2+}$ or $^*Fe^{3+}$ at the beginning of the Mössbauer transition following a single decay is equal to the capture-probability ratio on the central ion versus that on all possible electron acceptors other than the central ion,

$$r = \frac{\sigma_{^*Fe^{3+}}}{V \sum_i c_i \sigma_i}. \tag{1}$$

Here $\sigma_{^*Fe^{3+}}$ and σ_i are the electron-trapping cross sections of $^*Fe^{3+}$ and other acceptors of the lattice, respectively and c_i is the concentration of acceptor type i. V is the capture volume in

Table 1. Thermal history of the $LiNbO_3$ MES specimens and normalized Fe^{3+} fractions $R_{Fe^{3+}}$ as determined by the Fe^{3+} EPR intensity (reproducible to ± 0.05) on a reference crystal, which was heat treated together with the MES specimens.

	Fe doped or undoped			Mg doped or undoped	
Reduction state	B	D	E	H	I
Temperature (K)	1173	753	1073	1173	1073
Pressure (Pa)	10^5, air	2.5×10^{-4}	2.6×10^{-3}	10^5, O_2	2.9×10^{-3}
Time (h)	30	2	8	30	8
$R_{Fe^{3+}}$ (EPR)	1.00	0.52	0.00	1.00	0.22

which acceptors (of any kind) compete with the central ion in capturing the electrons *in the course of the last step* of the charge recombination. Assuming there is no charge relaxation in the lattice during the lifetime of the 14.4 keV nuclear level of ^{57}Fe, r in (1) can be related to the observed MES intensity ratio ${}^*R_{Fe^{3+}} = [{}^*Fe^{3+}]/([{}^*Fe^{2+}]+[{}^*Fe^{3+}])$ by $r = (1-{}^*R_{Fe^{3+}})/{}^*R_{Fe^{3+}}$. It is shown below that a carefully planned experiment can yield information on trapping cross sections and concentrations of the acceptors.

3. Experimental methods and results

Undoped, 0.1 mol% Fe and 5.4 mol% Mg *melt*-doped $LiNbO_3$ single crystals were grown in air from congruent melts (Li/Nb atomic ratio 0.94) from Merck Suprapure Li_2CO_3 and Starck Specpure Nb_2O_5 using a balance-controlled Czochralski method. X-ray oriented slices were cut from the boules and shaped separately. z-cut and y-cut slices of $(Fe_{0.001})LiNbO_3$ for electron paramagnetic resonance (EPR) and MES respectively, and y-cut for the other MES experiments. The platelets were chosen and controlled by ultraviolet (UV) absorption-edge measurements [22]. The $(Mg_{0.054})LiNbO_3$ platelet was 'threshold-doped', i.e. the absorption edge was at 310.8 nm, a value corresponding to a local minimum as a function of Mg melt-concentration [23]. Fe as a dopant was chosen in order to have an impurity of electron trapping cross section directly comparable with that of the central nucleogenic iron. This allows, as will be shown, to estimate the capture volume V from the experiment.

Fe and Mg containing crystals for MES and their parallel undoped specimens were dropped with 110 MBq and 18 MBq radioactive ^{57}Co respectively. Thermal diffusion of the ^{57}Co into the samples was carried out at 1173 K for 30 h, resulting also in complete oxidation of the crystals. The heat treatment was applied at atmospheric pressure in air for Fe-doped and in O_2 flow for Mg-doped samples.

Reduction heat treatment in vacuum is known to change the ferric/ferrous ratio of grown-in iron [24, 25] in a reproducible way. Subsequent oxidation/reduction heat treatments of the radioactive MES samples and one of the EPR samples were carried out in a common vacuum vessel with continuous pumping. The undoped and Fe-doped crystals turned dark grey in course of the reduction treatments. No darkening of the Mg-doped sample was observed. Since the change in ${}^*R_{Fe^{3+}}$ on reduction was small for $^{57}Co(Mg)LiNbO_3$, for this crystal only the oxidized and the fully reduced states are discussed here.

Table 1 illustrates the thermal history of $LiNbO_3$ specimens with capital letters representing the various thermochemical reduction (TCR) states of the crystals. The thermochemical states (A–I) of the crystals were characterized by the reduction state of the grown-in Fe impurity in an Fe-doped sample heat-treated with the MES specimens in the same vacuum vessel. The reduction state was determined by Fe^{3+} EPR intensity measurements.

Another Fe-doped reference crystal was set aside after the first oxidation heat treatment for Fe^{3+} EPR intensity reference. X-band EPR spectra were recorded by a JEOL FE3X spectrometer at room temperature. Adopting a method similar to that of Kurz *et al* [25], identically shaped unknown and reference crystals were mounted at exactly 90° on a sample holder attached to a goniometer. The $I_z = (-5/2) \rightleftharpoons (-3/2)$ transition of the Fe^{3+} ion in 1.1 T was recorded for the reference specimen in $H \parallel c$ geometry and the orientation was refined. Since there is no overlap of the $H_0 \parallel c$ and $H_0 \perp c$ EPR-spectra in this g-factor range, the Fe^{3+} signal could be separately recorded by turning the reference and unknown sample together by exactly 90°. By this method, with no need to change the sample or re-tune the cavity, we were able to reproduce the unknown to reference intensity ratio within 5%. The EPR intensities normalized to the Fe^{3+} intensity of the fully oxidized reference sample are deemed to represent the ferric fraction $[Fe^{3+}]/([Fe^{2+}] + [Fe^{3+}])$ of grown-in iron. These are the $R_{Fe^{3+}}$ values shown in the last row of table 1.

^{57}Co MES spectra were recorded at 4.2 K in a He-bath cryostat in an external magnetic field of 4.6 T parallel to the observation direction and perpendicular to the crystallographic c-axis. Source spectra of ^{57}Co:(Fe):$LiNbO_3$ crystals were analysed by a single line $Na_4[Fe(CN)_6] \cdot 10H_2O$ absorber containing 9 mg cm^{-2} natural Fe. MES measurements on Mg:$LiNbO_3$ were carried out using a methane gas-filled ^{57}Fe-enriched stainless steel resonance-detector. For velocity calibration a ^{57}Co:Fe source was used.

^{57}Co MES spectra without an external magnetic field show an unresolved $^*Fe^{3+}$ contribution (see figure 1) due to considerable relaxation effects [26]. However, 4.2 K MES spectra taken in an external magnetic field of 4.6 T are static, but the populations of low-lying electronic levels of $^*Fe^{3+}$ are out of thermal equilibrium [2, 3]. No relaxation takes place at 4.2 K within the Zeeman-split ground term [4]. $^*R_{Fe^{3+}}$ was determined in the following way. Due to the complexity of the Fe^{2+} spectrum in an external magnetic field, only Fe^{3+} was fitted, and the $^*Fe^{2+}$–$^*Fe^{3+}$ spectrum overlap region from -3.9 mm s^{-1} to +1.6 mm s^{-1} was excluded from the fit. The population of the sub-states of $^*Fe^{3+}$ is out of thermal equilibrium after the EC [2, 3], therefore no Boltzmann constraints were imposed on the relative intensities. The intensity of the $-1/2$ quartet which overlaps with the $^*Fe^{2+}$ pattern was taken to be equal to that of the $+1/2$ quartet, which is a good approximation for the $H_{ext} \perp c$ case [5].

Setting fit constraints for the quadrupole splitting ($QS = -0.243$ mm s^{-1} extracted from ^{57}Fe absorption Mössbauer measurements [27]) the obtained ^{57}Co MES parameters of the 5.4 mol% Mg:$LiNbO_3$ spectra are consistent with those described for congruent $LiNbO_3$ in the literature. The isomer shift (IS) relative to α-Fe at room temperature and the Fermi contact field per spin are $IS = 0.447 \pm 0.008$ mm s^{-1} and $H_c = 19.89 \pm 0.03$ T respectively. The Fe^{3+} line widths (constrained to be all equal in the fit) are almost equal to the apparative line width, no relaxation broadening is observed.

The nucleogenic Fe^{3+} fraction $^*R_{Fe^{3+}}$ was calculated by normalizing the summed up *fitted* intensity of the six $^*Fe^{3+}$ quartets (continuous line in figure 1) by the experimental integrated intensity. The statistical error of $^*R_{Fe^{3+}}$ is about 0.66% for undoped and Fe-doped and 0.75% for the Mg-doped $LiNbO_3$. Nucleogenic $^*Fe^{3+}$ fractions $^*R_{Fe^{3+}}$ are shown in table 2 and can be compared with the grown-in Fe^{3+} fractions $R_{Fe^{3+}}$ of table 1.

For the fully oxidized states B and H of undoped parallel samples the nucleogenic fraction $^*R_{Fe^{3+}}$ is reproduced well within the experimental error. While $R_{Fe^{3+}}$ varies in its full range ($1 > R_{Fe^{3+}} > 0$) on reduction, the change in $^*R_{Fe^{3+}}$ is remarkably limited. In accordance with the literature, only a minor change of $R_{Fe^{3+}}$ is observed on reduction in congruent $LiNbO_3$. The change on Fe doping is also weak, 0.1 mol% iron dopant only slightly modifies $^*R_{Fe^{3+}}$. In other words, Fe^{3+} *is not the dominant trap* in the capture volume. Consequently, there exist *intrinsic* electron traps in $LiNbO_3$ in the vicinity of the nucleogenic $^*Fe^{3+}$, which are very

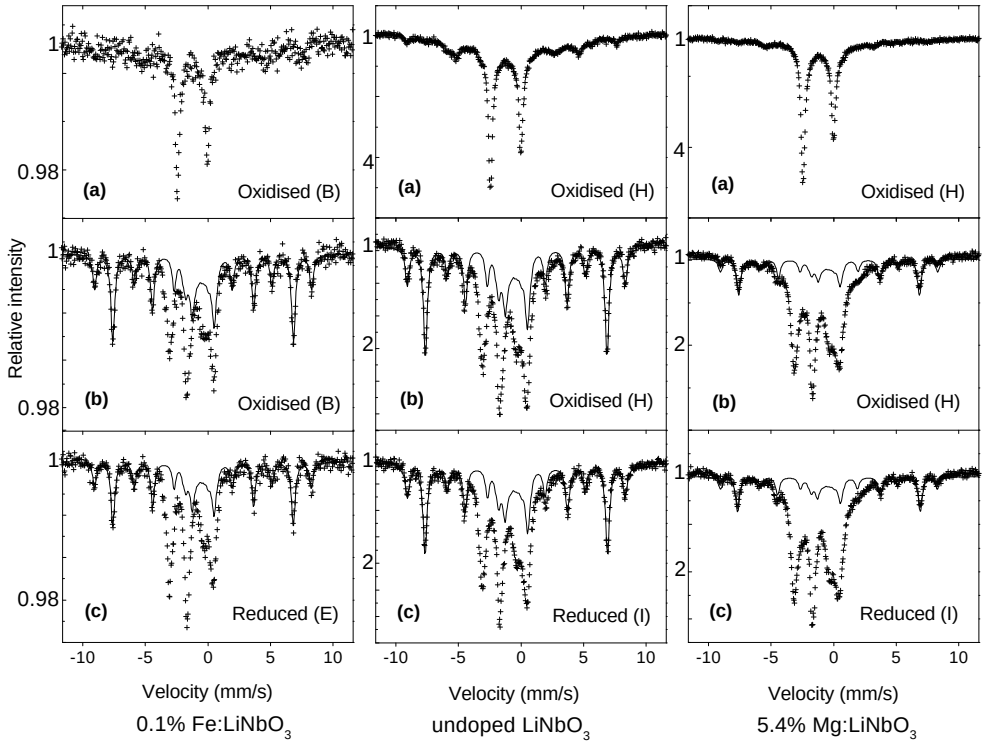

Figure 1. ^{57}Co MES spectra of $(Fe_{0.001})LiNbO_3$, undoped and $(Mg_{0.054})LiNbO_3$ at 4.2 K (a) without and (b), (c) with external magnetic field. The thermal treatment is indicated in brackets. Full lines are $^*Fe^{3+}$ fits described in the text. Resonance-detector spectra are inverted to facilitate comparison.

Table 2. Nucleogenic $^*Fe^{3+}$ fractions $^*R_{Fe^{3+}}$ measured by ^{57}Co MES for differently doped congruent $LiNbO_3$ crystals in various thermochemical states (A–I, see table 1).

Thermochemical state	B	D	E	H	I
$LiNbO_3$ 0.1% Fe	0.67	0.63	0.53	—	—
$LiNbO_3$ undoped	0.64	0.60	0.55	—	—
$LiNbO_3$ 5.4%Mg	—	—	—	0.33	0.30
$LiNbO_3$ undoped	—	—	—	0.64	0.59

effective and/or of high concentration, overshadowing the strong acceptor character of both Fe^{3+} and $^*Fe^{3+}$.

On reduction, the variation of $^*R_{Fe^{3+}}$ is somewhat larger for the 0.1 mol% Fe-doped than for undoped $LiNbO_3$ crystal, indicating a small but non-negligible acceptor effect of the grown-in iron. Mg doping, however, drastically influences $^*R_{Fe^{3+}}$. As far as we know, this is the first evidence that the nucleogenic ratio $r = [^*Fe^{2+}]/[^*Fe^{3+}]$ could be considerably modified by changing the properties of the $LiNbO_3$ matrix.

In order to describe the charge relaxation of and around a nucleogenic iron ion, the possible electron traps of the lattice (including the observed central ion), as well as their concentration and trapping efficiencies, have to be considered.

4. Discussion

4.1. Intrinsic and extrinsic defects in congruent $LiNbO_3$

Information on intrinsic defects in congruent $LiNbO_3$ is somewhat controversial. However, all current defect models of the as-grown state agree that part of the Li sites are filled up by excess Nb^{5+} ions to accommodate Li deficiency. For reasons of the charge misfit these Nb_{Li} antisites are strong electron traps and are situated near or inside defective regions, though their nature is still debated [28–33].

In the original model of Lerner *et al* [28, 31, 32], each Nb_{Li} antisite is compensated by four lithium vacancies which are potential hole traps. The number of antisites in the crystal can be estimated from our Li/Nb melt ratio (0.940) to be 1.0(1) mol% (1.0 ± 0.1 mol%). In the later model of Smyth [29, 30, 34] the lithium vacancies are replaced by ($Nb^{5+}_{Li\square Nb}$) complexes, which are simply restructured lithium vacancies and behave as hole traps [30]. (The $\square$ stands for a vacancy, the subscript denotes the 'original' site occupancy and the superscript the absolute formal charge of the species.) This model uses the low stability of the lithium niobate lattice against reversals in the –Li–Nb–Li–Nb– stacking order (along the crystal *c* axis), which might result in –Nb–Li–Li–Nb– stacked non-ferroelectric regions. The over-compensated Nb^{5+}_{Li} antisites formally present in these ($Nb^{5+}_{Li\square Nb}$) complexes should therefore not be considered as real antisites.

ESR results on x- or γ-irradiated crystals [35, 36], or on thermochemically reduced and subsequently UV-irradiated samples [37], show a single type of filled electron trap centre (together with only one type of a hole centre in irradiated crystals). This centre has concentrations of the order of up to 1 mol%, and can be assigned, together with an absorption band at 1.6 eV, to antisites in the Nb^{4+} charge state.

On thermochemical reduction oxygen leaves the crystal, elementary cells are lost on the surface, the cations migrate and fill up cation vacancies:

$$2LiNbO_3 + 4\square_{Li} \leftrightarrow 3O_2 + 2Li_{Li} + 2Nb_{Li} + 12e^- \qquad (2a)$$

$$2LiNbO_3 + 4(Nb_{Li\square Nb}) \leftrightarrow 3O_2 + 2Li_{Li} + 2Nb_{Li} + 4Nb_{Nb} + 12e^- \qquad (2b)$$

the two variants corresponding to the models of Lerner and Smyth, respectively. Electrons left behind get trapped on Nb_{Li} antisites, preferentially on the freshly formed uncompensated antisites but also on the as grown ones not shown in (2*a*) and (2*b*). In fact, due to diffusion of the charge compensators the difference between the various antisites tends to disappear. As indicated by the rather weak Nb^{4+} ESR signals in as-reduced crystals [37], trapping occurs preferentially pairwise, forming bipolarons involving a Nb_{Li} and a nearest neighbour regular Nb_{Nb} site [34, 38]. As shown by Schirmer *et al* [37], the diamagnetic bipolarons represent the ground state of the reduced crystal, which can be excited by UV illumination to a state where bipolarons are dissociated and large numbers of antisites in the paramagnetic Nb^{4+} polaron state can be observed [37]. This means that in reduced crystals, similar to as-grown ones, only one type of active electron trap, the Nb_{Li} antisites, are present. The number of these empty electron traps is smaller in reduced than in as-grown crystals, since, assuming exclusively pairwise trapping, 8 out of the 12 electrons in (2*a*) and (2*b*) are used up to fill four as-grown antisites, two-thirds per outdiffused oxygen atom. All these statements are independent of the intrinsic defect model chosen. Oxygen vacancies, earlier believed to play a major role in electron trapping, are today known to be practically absent [34, 39].

In concentrations of up to a few percent, Fe [40–42] and Mg [39, 43] substitute for Li. Similar behaviour is concluded for Co from EXAFS measurements [44]. On a theoretical basis, Donnerberg *et al* [30] conclude that incorporation of most divalent and trivalent impurity ions (including Co^{2+} and Fe^{3+}) simply means the replacement of intrinsically present Nb_{Li} antisite

traps by impurity ion traps with different trapping efficiency. These cation impurities may be compensated by the same intrinsic hole trap defects, only in smaller numbers, as the Nb_{Li} antisites. As shown by EPR, the overwhelming majority of Co^{2+} and Fe^{3+} defects have local axial symmetry indicating that possible charge compensator(s) are either along the *c* axis or outside the nearest-neighbour spheres (for a summary and references see [34]).

The Mg impurity in $LiNbO_3$ has additional features and behaves in a somewhat different manner than Fe^{3+} and Co^{2+}. Heavily Mg-doped $LiNbO_3$ crystals show remarkable photo-conductivity short-circuiting the space charges which otherwise would cause the photorefractive effect [45]. This effect exhibits a distinct threshold at a critical concentration $[Mg]_c \geqslant 4.5$ mol% (in the congruent melt) with several other properties also exhibiting abrupt changes at $[Mg]_c$ [34]. It has been established that this Mg-concentration threshold is related to a *complete* elimination of the strong intrinsic electron traps, the Nb_{Li} antisites [34, 38]. Electron traps associated with Mg impurities are assumed to be very shallow [46] and delocalized [47].

Due to their high formation energy [34], oxygen vacancies are not likely to form during the Auger process following the EC. In the following, we will make extensive use of the fact, that hole mobility at room temperature is about 200 times smaller than electron mobility [48]. Consequently, thermal de-trapping and/or diffusion of holes, i.e. any role of hole traps in the charge-recombination processes relevant to our 4.2 K temperature MES can be ignored.

In accordance with the experimental results and the discussed defect models, the relevant traps for our MES experiments are the following: a single electron trap, namely Nb_{Li}, in undoped $LiNbO_3$; two distinct electron traps, namely Nb_{Li} and Fe_{Li}^{3+} in $(Fe_{0.001})LiNbO_3$ and a single shallow Mg-related defect in threshold-doped $(Mg)LiNbO_3$. These electron traps compete with the nucleogenic iron in re-capturing electrons generated in the course of the Auger process. Due to the low mobility of holes the observed $[^*Fe^{2+}]/[^*Fe^{3+}]$ ratio is determined by the interplay between the observed nucleogenic ion and the electron traps in the capture volume around this ion, taking into account the time window determined by the lifetime of the Mössbauer level of ^{57}Fe.

For undoped $LiNbO_3$ (table 2), the variation of $^*R_{Fe^{3+}}$ on reduction is linear (on a scale defined by $R_{Fe^{3+}}$, the ferric fraction of the $(Fe_{0.001})LiNbO_3$ non-radioactive reference crystal, cf table 1). In contrast, in $(Fe_{0.001})LiNbO_3$, $^*R_{Fe^{3+}}$ shows a nonlinear evolution on reduction. Consequently, while charge trapping in undoped $LiNbO_3$ can be modelled with a single kind of intrinsic electron trap, at least two kinds of electron traps have to be considered in $(Fe_{0.001})LiNbO_3$ as discussed above.

The larger variation of $^*R_{Fe^{3+}}$ on reduction in $(Fe_{0.001})LiNbO_3$ (with respect to the undoped crystal) indicates that Fe^{3+} is a more efficient electron acceptor than the intrinsic defect in undoped $LiNbO_3$. Using the discussed defect models, below we present a simple competing acceptors model of the electron trapping following the EC of ^{57}Co in $LiNbO_3$.

4.2. Electron capture in undoped and Fe-doped congruent $LiNbO_3$

In the following we shall estimate the capture volume *V* of the recombination cascade following the EC in $LiNbO_3$, as well as the ratios of the cross sections of the various electron traps using our experimental data. As a first step we consider the undoped and Fe-doped $LiNbO_3$ crystals in their completely oxidized state. We assume a single kind of intrinsic acceptor of cross section σ_{in} in undoped $LiNbO_3$ and the same kind of intrinsic acceptor in $(Fe_{0.001})LiNbO_3$. Neglecting trapping on impurities and crystal defects other than Fe^{3+}, the nucleogenic $[^*Fe^{2+}]/[^*Fe^{3+}]$ ratios observed in undoped $LiNbO_3$ and $(Fe)LiNbO_3$ (r^u and r^{Fe}, respectively) are (see (1))

$$r^u = \frac{\sigma_{^*Fe^{3+}}}{V c_{in}^u \sigma_{in}} \tag{3}$$

and

$$r^{\mathrm{Fe}} = \frac{\sigma_{{}^{*}\mathrm{Fe}^{3+}}}{V(c_{\mathrm{in}}^{\mathrm{Fe}}\sigma_{\mathrm{in}} + c_{\mathrm{Fe}}R_{\mathrm{Fe}^{3+}}\sigma_{\mathrm{Fe}^{3+}})}. \tag{4}$$

Here $c_{\mathrm{in}}^{\mathrm{u}}$ and $c_{\mathrm{in}}^{\mathrm{Fe}}$ are the concentrations of intrinsic acceptors in undoped and Fe-doped $LiNbO_3$, respectively. The concentration of grown-in iron is c_{Fe}, out of which a fraction of $R_{\mathrm{Fe}^{3+}}$, as measured by EPR, is in the ferric (active trap) state and $R_{\mathrm{Fe}^{2+}} = 1 - R_{\mathrm{Fe}^{3+}}$ in the Fe^{2+} (inactive trap) state. In (4) we neglected trapping of electrons by ${}^{*}Fe^{2+}$ ($\sigma_{\mathrm{Fe}^{2+}} = 0$) since no ${}^{*}Fe^{1+}$ has ever been observed in MES of $LiNbO_3$. Now if we assume that trapping cross sections of nucleogenic ${}^{*}Fe^{3+}$ and grown-in Fe^{3+} are equal $\sigma_{{}^{*}\mathrm{Fe}^{3+}} = \sigma_{\mathrm{Fe}^{3+}}$ we can determine $\sigma_{\mathrm{Fe}^{3+}}/\sigma_{\mathrm{in}}$ and V, and thereby the electron capture radius from (3) and (4) provided that $c_{\mathrm{in}}^{\mathrm{u}}$ and $c_{\mathrm{in}}^{\mathrm{Fe}}$ are known. This is, in fact, well established for the oxidized state of $LiNbO_3$ in frames of the discussed defect models identifying the intrinsic traps with antisite Nb_{Li}^{5+}.

Admittedly, it can hardly be excluded that the trapping cross sections of nucleogenic ${}^{*}Fe^{3+}$ and grown-in Fe^{3+} are somewhat different for the following reason. The mother isotope of the nucleogenic iron is ^{57}Co the original state of which after diffusion is Co^{2+}. Therefore the average charge compensation of the two iron species may be somewhat different. While the average charge compensation is certainly typical for a trivalent ion in the case of grown-in Fe^{3+}, it may be closer to that of a divalent ion in the case of nucleogenic ${}^{*}Fe^{3+}$. Nevertheless, as we shall see immediately, this difference has very little influence on the value of the capture radius. To describe the possible difference in the cross sections we introduce the factor q

$$\sigma_{{}^{*}\mathrm{Fe}^{3+}} = q\sigma_{\mathrm{Fe}^{3+}}. \tag{5}$$

For a rough estimate of q one may assume that the cross section is proportional to the excess charge of the ion, which yields $q \sim 2$ as a more conservative assumption we shall use $1 < q < 10$. Since r^{u}, r^{Fe} and $R_{\mathrm{Fe}^{3+}}$ are measured, one can now determine $\sigma_{\mathrm{Fe}}/\sigma_{\mathrm{in}}$ and V/q from (3) and (4). As mentioned above, incorporation of Fe^{3+} decreases the concentration of antisite Nb_{Li}^{5+} at this doping level. For charge compensation reasons, for each incorporated Fe^{3+} ion only 0.6 Nb_{Li}^{5+} ions are replaced [30], i.e. for the fully oxidized state, $c_{\mathrm{in}}^{\mathrm{u}} = 1.0$ mol% and $c_{\mathrm{in}}^{\mathrm{Fe}} = c_{\mathrm{in}}^{\mathrm{u}} - 0.6\,c_{\mathrm{Fe}}$. Using the experimental data for r^{u}, r^{Fe} and $R_{\mathrm{Fe}^{3+}}$, (3) and (4) can be solved yielding: $\sigma_{\mathrm{Fe}}/\sigma_{\mathrm{in}} = 2.0 \pm 0.7$ and $V/q = 19 \pm 9$ nm^3, respectively.

In accordance with the expectation and experimental results [20], Fe^{3+} is an electron trap of larger trapping cross section than the intrinsic Nb_i. Assuming a spherical capture volume and $1 < q < 10$, a capture radius of 2.7 ± 1.4 nm is found, where $q = 2$ corresponds to 2.1 nm. This is significantly larger than a first-neighbour effect (according to the auto-radiolysis model [12]) would require, but it is much smaller than the mean free path of the ~6 keV Auger electrons (~100 nm [21]). Therefore charge trapping by Fe^{3+} is much more *local* than believed before [19, 20]. Only those electrons which are in a distance of a few unit cells seem to compete with the central ion in the course of the ${}^{*}Fe^{3+} \rightarrow {}^{*}Fe^{2+}$ charge relaxation. This local character of the capture was already pointed out in a preliminary stage of the present study [7]. The origin of this effect is the following. The estimated average energy of an electron–hole pair is three to four times the band gap [10]. Taking a branching ratio of 1.3 [10] for 6 keV to 600 eV Auger electrons, more than one order of magnitude less electron–hole pairs are created by the ~600 eV Auger electrons than by the 6 keV Auger electrons. Nevertheless, the penetration range of the lower energy Auger electrons in $LiNbO_3$ is about 11 nm, a value about 22 times smaller than that for the ~6 keV electrons [21]. Therefore the concentration of electrons generated by the ~600 eV LMM Auger electrons in the close environment of the nucleogenic ion is still about *four orders of magnitude higher* than those generated by the ~6 keV Auger electrons. The electrons in the capture volume provided by the lattice for the charge relaxation therefore almost exclusively originate from the ~600 eV LMM Auger cascade.

4.3. Electron capture in congruent Mg:$LiNbO_3$

The measured nucleogenic $^*Fe^{3+}$ fraction is reduced by about a factor of two (from 0.64 to 0.33) in the threshold-doped Mg:$LiNbO_3$ crystal. This shows that Mg considerably reduces the electron trapping efficiency of the matrix, but *there still exists* certain type(s) of electron acceptor(s) in this lattice. These extrinsic traps (of concentration c_{ex}^{Mg} and of cross section σ_{Mg}) are, in some way, related to Mg. However, they are certainly *not* Nb_{Li} antisites, since at this Mg concentration no Nb_{Li} was observed in the EPR and optical spectra of irradiated or reduced samples [34, 36]. At the concentration threshold near 5 mol% all Nb_{Li} antisites are eliminated [39] and after reduction a different trapped electron centre is observed [36], attributed to a $Mg_{Li}^{2+}Nb_{Nb}^{4+}$ defect complex [47]. Over-threshold doping may increase the Mg_{Li} concentration, but only slowly since the excess Mg substitutes on both Li *and* Nb sites. This latter species forms Mg_{Nb} hole traps [49] which will be excluded from charge relaxation considerations for reasons mentioned earlier. Other hole traps such as isolated Li vacancies will be ignored for the same reason. Consequently, for threshold-doped Mg:$LiNbO_3$ again a single-trap model can be applied

$$r^{Mg} = \frac{q\sigma_{Fe^{3+}}}{V c_{ex}^{Mg}\sigma_{Mg}}. \tag{6}$$

The concentration of the extrinsic electron traps may be assumed to be equal to the Mg concentration ($c_{ex}^{Mg} = 5.4$ mol%). As we shall see in the next section, this may be an overestimate, as a substantial part of the $Mg^{+}Nb_{Nb}^{5+}$ complexes may be closely associated with a charge compensating lithium vacancy [34, 39], making the complexes inactive as electron traps. With the assumption that the capture volume is the same for undoped and Mg-doped $LiNbO_3$, one finds $\sigma_{Fe}/\sigma_{Mg} = 39 \pm 11$, showing a large difference in the electron-trapping cross sections of the Mg_{Li} centre and Fe^{3+}. The ratio $\sigma_{in}/\sigma_{Mg} = 19 \pm 7$ can also be derived from the above results. Even if these values are overestimates by a factor of 2–3, these proportions readily explain the considerably increased photoconductivity observed by holographic erasure time measurements in threshold Mg-doped crystals [45] and imply a shallow Mg_{Li} trap.

4.4. Trap model applied to the thermochemically reduced states of $LiNbO_3$

First we discuss the case of pure and Fe-doped crystals, then the case of Mg-doped $LiNbO_3$. As discussed in section 4.1, in undoped $LiNbO_3$, Nb_{Li}^{5+} centres remain the major electron traps after reduction, and part of them, not filled by bipolarons or polarons during reduction, will be active during the MES experiment. In the case of the $(Fe_{0.001})LiNbO_3$ crystal the respective Fe^{3+} fraction given in table 1 also has to be considered. Under the conditions of the MES experiment (much lower temperatures and extremely short times as compared to reduction) only single trapping processes seem to be important. Again, the same trapping models can be applied. Using (3)–(6) and the trap parameters found for the fully oxidised crystals, one can also draw conclusions for the reduced state of $LiNbO_3$. Provided that no significant change occurs in the capture volume and the trapping cross sections on reduction, the concentration of the electron traps can be derived for the various reduced states as given in table 3.

Errors in concentrations are ± 0.33 mol% for $c_{in}^{u,Fe}$. Note that these are the concentrations of *active* (i.e. empty) electron traps of the lattice. The concentration of traps depends on how many of them are filled during the thermochemical reduction. The number of active traps lost during reduction can readily be obtained by subtracting the values in table 3 from the initial concentrations corresponding to fully oxidized states, i.e. 1.0, 0.94 and 5.4 mol% for c_{in}^{u}, c_{in} and c respectively. As follows from the discussion in section 4.1, during reduction of the undoped crystal each leaving oxygen atom fills two-thirds as-grown antisites with electrons,

Table 3. Active acceptor concentrations c_{in}^{u}, $c_{\text{in}}^{\text{Fe}}$ and $c_{\text{ex}}^{\text{Mg}}$ (mol%) of reduced $LiNbO_3$. The reduction state is ranked based on the $R_{Fe^{3+}}$ values from table 1.

Parameter	Thermochemical state	D	I	E
c_{in}^{u}	undoped $LiNbO_3$	0.84	0.81	0.69
$c_{\text{in}}^{\text{Fe}}$	$(Fe_{0.001})LiNbO_3$	0.85	—	0.63
$c_{\text{ex}}^{\text{Mg}}$	$(Mg_{0.054})LiNbO_3$	—	4.70	—

if only bipolaron trapping is taken into account, and somewhat more if the smaller trapped polaron fraction is also considered. The number of oxygen molecules leaving the crystal can thus be estimated. Assuming only bipolaron production, for the fully reduced state, E, this yields a weight loss $\Delta = 0.050$ wt%, (or somewhat less if polaron trapping is also taken into account), which is in reasonable agreement with 0.0326 ± 0.0015 wt% measured by Holmes, as reported by Smyth [29], for samples reduced for an unspecified time at 1050 °C in 10^{-7} Pa of O_2. Since the reduction conditions are slightly different for the two measurements, these results cannot be compared directly.

Physical properties of $LiNbO_3$ reproduce on oxidation–reduction treatments. However, a proper characterization of a certain thermochemical state of the crystals is extremely difficult. This is the reason why the parameter $R_{Fe^{3+}}$ was chosen for this purpose here. In view of the MES results we can check to what extent the reduction state of $LiNbO_3$ is followed by that of Fe ($Fe^{3+} \rightleftharpoons Fe^{2+}$). The concentration of the grown-in Fe varies in its full range $Fe^{3+} \rightleftharpoons Fe^{2+} (0 < R_{Fe^{3+}} < 1)$ between states B to E, but state E is certainly not the 'most reduced' state possible for the lattice. About two-thirds of the intrinsic acceptors are still present in the lattice (see table 3). A total reduction of the matrix would mean elimination of *all* active Nb_{Li} antisites. As a consequence of the different trapping efficiencies for Fe^{3+} and Nb_i, ${}^*R_{Fe^{3+}}$ shows a nonlinear evolution on $R_{Fe^{3+}}$. Whether or not the nucleogenic ${}^*R_{Fe^{3+}}$ fraction is a more suitable 'scale' for the characterization of the thermochemical state of $LiNbO_3$ can be decided by the MES result on a stoichiometric $LiNbO_3$.

Equation (2) is no longer valid for threshold Mg-doped $LiNbO_3$, and unfortunately we do not have an established defect model for the reduction of this material. It is very likely that the concentration of Mg_{Li} remains constant on reduction. As the simplest model of reduction we suggest the following: every effused oxygen atom leaves two electrons behind, which get trapped on two ($Mg_{Li}Nb_{Nb}$) complexes, as no other electron traps are present. The change in the acceptor concentration on reduction (B–I) calculated for $(Mg_{0.054})LiNbO_3$ assuming all ($Mg_{Li}Nb_{Nb}$) complexes to be active, is 0.69 mol%, which is more than three times higher than the change in the parallel undoped $LiNbO_3$ sample (0.19 mol%), corresponding to a slightly larger or comparable oxygen loss in $(Mg)LiNbO_3$. As this contrasts to the experience that oxygen effusion from threshold Mg-doped $LiNbO_3$ is more difficult than from congruent ones [34], one has to assume that the majority of ($Mg_{Li}Nb_{Nb}$) complexes are inactive. This may be due to partial charge compensation of the complexes by lithium vacancies (see section 4.3).

5. Conclusions and final remark

Mössbauer emission spectroscopic measurement of the nucleogenic ferric fraction ${}^*R_{Fe^{3+}}$ following the EC of ^{57}Co in undoped congruent, 0.1 mol% Fe-doped and overthreshold-doped $(Mg_{0.054})LiNbO_3$ single crystals was presented. Charge relaxation of the matrix following the energetic Auger cascade can be described by Nb_{Li} antisites being the dominant intrinsic acceptors in undoped and weakly Fe-doped $LiNbO_3$. The same role is apparently

played by uncompensated $Mg_{Li}Nb_{Nb}$ complexes representing a fraction of the Mg dopants in overthreshold Mg-doped $LiNbO_3$ crystals. Fe^{3+}_{Li} is found to be a stronger electron trap in $LiNbO_3$ than Nb^{5+}_{Li} by a factor of $\sigma_{Fe}/\sigma_{in} = 2.0 \pm 0.7$, and far stronger than the trap related to Mg.

Acceptor concentrations for TCR states of $LiNbO_3$ have also been derived. Within the frame of a defect model, the reduction balance was investigated, including the quantity of oxygen effused from the lattice.

The TCR state of Fe, as followed by EPR, does not provide a linear scale for the characterization of the intrinsic reduction state of the $LiNbO_3$ lattice, since iron is only the minority acceptor among traps with different cross sections.

The model of competing acceptors is found to be valid in the crystals studied, although trapping is much more local than believed earlier. The capture radius for $^*Fe^{3+}$ is 2.7 ± 1.4 nm. The major source of charge carriers contributing to the charge relaxation of the nucleogenic iron are the quasi-free electron-polarons generated by the emission of $\sim$600 eV LMM Auger electrons, a feature independent of the studied matrix.

Finally we should like to remark that measurements of intrinsic electron–hole recombination processes in electron irradiated crystals from the same source have recently been started by observing time resolved luminescence and induced absorption. Preliminary results [50] show complex decay behaviour with the largest portion of electron–hole pairs or excitons decaying faster than 20 ns, while the rest decays on much slower microsecond time scales, depending also on temperature. In congruent crystals only fast luminescence is observed. This is in overall agreement with the Mössbauer results of the paper.

Acknowledgments

Helpful discussions with Professor A Rockenbauer are gratefully acknowledged. Thanks are due to Dr B Molnár and Mr F Gazdácska for the radiochemical work. This work was partly supported by the Hungarian Scientific Research Fund (OTKA) under contract nos T022145 and 24092, and by the NATO Collaborative Research Grant no HTECH.CRG 930478. One of the authors (T B-D) was supported by a scholarship of the Hungarian Ministry of Culture and Education.

References

[1] Keune W, Date S K, Dézsi I and Gonser U 1975 *J. Appl. Phys.* **46** 3914
[2] Doerfler R, Nagy D L, Pfannes H-D, Putzka A, Ritter G and Zeman N 1984 *Phys. Status Solidi* b **124** 767
[3] Doerfler R *et al* 1986 *Phys. Rev. Lett.* **57** 2849
[4] Gruber W, Nagy D L, Ritter G and Szücs I S 1988 *Hyperfine Interact.* **42** 1043
[5] Tuczek F 1988 *PhD Thesis* Universität Mainz, p 176
[6] Leupold O, Billenstein M, Giesse E, Gruber W, Molnár B, Nagy D L, Ritter G and Röhlich U 1990 *Hyperfine Interact.* **56** 1539
[7] Sayed S, Bottyán L, Becze-Deák T, Nagy D L, Korecz L, Polgár K and Spiering H 1995 *XXX Zakopane School of Physics Proc.* ed K Tomala and E A Görlich (Krakow: Institute of Physics) p 428
[8] Helms W R and Mullen J G 1971 *Phys. Rev.* B **4** 750
[9] Bondarevskii S I, Tarasov V A and Shcherbakov E E 1973 *Radiochimiya* **15** 897
[10] Spiering H, Alflen M, Gütlich P, Hauser A, Hennen C, Manthe U and Tuczek F 1990 *Hyperfine Interact.* **53** 113
[11] Pollak H 1962 *Phys. Status Solidi* **2** 720
[12] Friedt J M and Danon J 1980 *At. Energy Rev.* **18** 893
[13] Goldanskii V I and Stukan R A 1980 *J. Physique* **41** C1–43
[14] Nagy D L 1983 *Second Seeheim Workshop: Trends in Mössbauer Spectroscopy Proc. (Mainz, 1983)* ed P Gütlich and G M Kalvius p 241

[15] Spiering H, Alflen M, Hennen C, Kajcsos Zs, Tuczek F and Gütlich P 1991 *XXVI Zakopane School of Physics Proc.* ed J Stanek and T Pedziwiatr (Singapore: World Scientific Publisher) p 199
[16] Nagy D L 1994 *Hyperfine Interact.* **83** 3
[17] Tuczek F, Spiering H and Gütlich P 1990 *Phys. Rev.* B **41** 10 933
[18] Wertheim G K 1961 *Phys. Rev.* **124** 764
[19] Tejada J and Parak F 1981 *Hyperfine Interact.* **10** 1227
[20] Harami T, Loock J, Huenges E, Fontcuberta J, Obradors X, Tejada J and Parak F 1984 *J. Phys. Chem. Solids* **45** 181
[21] Siegbahn K 1955 *Beta and Gamma-Ray Spectroscopy* ed K Siegbahn (Amsterdam: Elsevier) p 23
[22] Kovács L, Ruschhaupt G, Polgár K, Corradi G and Wöhlecke M 1997 *Appl. Phys. Lett.* **70** 2801
[23] Polgár K, Kovács L, Földvári I and Cravero I 1986 *Solid State Commun.* **59** 375
[24] Peterson G E, Glass A M and Negran T J 1971 *Appl. Phys. Lett.* **19** 130
[25] Kurz H, Krätzig E, Keune W, Engelmann H, Gonser U, Dischler B and Räuber A 1977 *Appl. Phys.* **12** 355
[26] Pfannes H-D and Putzka A 1983 *Hyperfine Interact.* **15/16** 837
[27] Putzka A and Pfannes H-D 1982 *Appl. Phys.* A **29** 1
[28] Lerner P, Legras C and Dumas J 1968 *J. Cryst. Growth* **3–4** 231
[29] Smyth D M 1983 *Ferroelectrics* **50** 93
[30] Donnerberg H, Tomlinson S M, Catlow C R A and Schirmer O F 1989 *Phys. Rev.* B **40** 11 909
[31] Iyi N, Kitamura K, Izumi F, Yamamoto J K, Hayashi T, Asuno H and Kitamura S 1992 *J. Solid State Chem.* **101** 340
[32] Zotov N, Boysen H, Frey F, Metzger T and Born E 1994 *J. Phys. Chem. Solids* **55** 145
[33] Leroux C, Nihoul G, Malovichko G I, Grachev V G and Boulesteix C 1998 *J. Phys. Chem. Solids* **59** 311
[34] Schirmer O F, Thiemann O and Wöhlecke M 1991 *J. Phys. Chem. Solids* **52** 185
[35] Schirmer O F and von der Linde D 1978 *Appl. Phys. Lett.* **33** 35
[36] Sweeney K L, Halliburton L E, Bryan D A, Rice R R, Gerson R and Tomaschke H E 1985 *J. Appl. Phys.* **57** 1036
[37] Ketchum J L, Sweeney K L, Halliburton L E and Armington A F 1983 *Phys. Lett.* A **94** 450
[38] Donnerberg H, Tomlinson S M and Catlow C R A 1991 *J. Phys. Chem. Solids* **52** 201
[39] Donnerberg H, Tomlinson S M, Catlow C R A and Schirmer O F 1991 *Phys. Rev.* B **44** 4877
[40] Rebouta L, da Silva M F, Soares J C, Hage-Ali M, Stoquert J P, Siffert P, Sany-García J A, Diéguez E and Agulló-López F 1991 *Europhys. Lett.* **14** 557
[41] Prieto C and Zaldo C 1992 *Solid State Commun.* **83** 819
[42] Söthe H and Spaeth J M 1992 *J. Phys.: Condens. Matter* **4** 9901
[43] Bush T S, Catlow C R A, Chadwick A V, Cole M, Geatches R M, Greaves G N and Tomlinson S M 1992 *J. Mater. Chem.* **2** 309
[44] Catlow C R A, Chadwick A V, Cole M and Tomlinson S M 1991 *Radiat. Eff. Defects Solids* **119–121** 565
[45] Bryan D A, Gerson A and Tomaschke H E 1984 *Appl. Phys. Lett.* **44** 847
[46] Koppitz J, Kuznetsov A I, Schirmer O F, Wöhlecke M, Wörner R and Grabmaier B C 1988 *Proc. SPIE* **1018** 23
[47] Zaritskii I M, Rakitina L G and Polgár K 1995 *Fiz. Tverd. Tela* **37** 1970 (Eng. Transl. 1995 *Phys. Status Solidi* **37** 1073)
[48] Krätzig E 1978 *Ferroelectrics* **21** 635
[49] Zaritskii I M, Rakitina L G, Corradi G, Polgár K and Bugai A A 1991 *J. Phys.: Condens. Matter* **3** 8457
[50] Grigorjeva L, Millers D, Corradi G, Polgár K and Pankratov V *EURODIM'98 Conf. (Keele, UK)* to be published